

Elemental separation in nanocrystalline Cu-Al alloys

Cite as: Appl. Phys. Lett. **102**, 231912 (2013); <https://doi.org/10.1063/1.4811157>

Submitted: 10 April 2013 • Accepted: 30 May 2013 • Published Online: 12 June 2013

Y. B. Wang, X. Z. Liao, Y. H. Zhao, et al.



View Online



Export Citation



CrossMark

ARTICLES YOU MAY BE INTERESTED IN

[Tailoring stacking fault energy for high ductility and high strength in ultrafine grained Cu and its alloy](#)

Applied Physics Letters **89**, 121906 (2006); <https://doi.org/10.1063/1.2356310>

[Dislocation density evolution during high pressure torsion of a nanocrystalline Ni-Fe alloy](#)

Applied Physics Letters **94**, 091911 (2009); <https://doi.org/10.1063/1.3095852>

[Formation mechanism of fivefold deformation twins in nanocrystalline face-centered-cubic metals](#)

Applied Physics Letters **86**, 103112 (2005); <https://doi.org/10.1063/1.1879111>

 QBLOX



1 qubit

Shorten Setup Time

Auto-Calibration

More Qubits

Fully-integrated

Quantum Control Stacks

Ultrastable DC to 18.5 GHz

Synchronized <<1 ns

Ultralow noise



100s qubits

[visit our website >](#)

Elemental separation in nanocrystalline Cu-Al alloys

Y. B. Wang,¹ X. Z. Liao,^{1,a)} Y. H. Zhao,² J. C. Cooley,³ Z. Horita,⁴ and Y. T. Zhu^{5,a)}

¹*School of Aerospace, Mechanical and Mechatronics Engineering, The University of Sydney, Sydney, NSW 2006, Australia*

²*School of Materials Science and Engineering, Nanjing University of Science and Technology, Nanjing 210094, China*

³*Division of Materials Science and Technology, Los Alamos National Laboratory, Los Alamos, New Mexico 87545, USA*

⁴*WPI, International Institute for Carbon-Neutral Energy Research (WPI-I2CNER), Kyushu University, Fukuoka 819-0395, Japan*

⁵*Department of Materials Science and Engineering, North Carolina State University, Raleigh, North Carolina 27695, USA*

(Received 10 April 2013; accepted 30 May 2013; published online 12 June 2013)

Nanocrystallization by high-energy severe plastic deformation has been reported to increase the solubility of alloy systems and even to mix immiscible elements to form non-equilibrium solid solutions. In this letter, we report an opposite phenomenon—nanocrystallization of a Cu-Al single-phase solid solution by high-pressure torsion separated Al from the Cu matrix when the grain sizes are refined to tens of nanometers. The Al phase was found to form at the grain boundaries of nanocrystalline Cu. The level of the separation increases with decreasing grain size, which suggests that the elemental separation was caused by the grain size effect. © 2013 AIP Publishing LLC. [<http://dx.doi.org/10.1063/1.4811157>]

Severe plastic deformation (SPD) techniques including equal channel angular pressing and high-pressure torsion (HPT) have been widely used to refine the grain sizes of metallic materials for superior mechanical properties.^{1,2} Recent detailed structural investigations of materials processed by SPD revealed that SPD processing resulted in complicated structural evolution of materials that include grain refinement,^{3,4} grain growth when the starting grain sizes in the materials are very small,^{5,6} phase transformation,^{7,8} and elemental redistribution that could also result in a phase transformation.^{9,10} One significant phenomenon that has been widely reported is that nanocrystallization by mechanical alloying could mix immiscible elements to form solid solutions.^{11–17}

In this letter, we report an opposite phenomenon that nanocrystallization by HPT separated Al from originally equilibrium single-phase Cu-Al solid solutions when the grain sizes of the materials are refined to a few tens of nanometers. The phenomenon was first discovered in HPT-processed commercially pure Cu and was confirmed in carefully prepared Cu-5 at. % Al and Cu-10 at. % Al alloys, although a Cu-Al alloy with the Al content of less than 18 at. % should form a single face-centred cubic Cu(Al) solid solution.¹⁸

The Cu-5 at. % Al and Cu-10 at. % Al alloys used in this investigation were prepared by arc-melting 99.9999% pure (metals basis) elemental copper and aluminium in a zirconium gettered argon atmosphere. X-ray diffraction data confirmed that the as-cast Cu-Al alloys are of a face-centred cubic crystal structure, i.e., the alloys are single-phase Cu (Al) solid solutions. The grain sizes in the as-cast samples are usually several microns. Room temperature HPT processing was conducted on

disks with a diameter of ~ 10 mm and a thickness of ~ 1 mm under a pressure of 6 GPa for 5 revolutions. Transmission electron microscopy (TEM) characterization was carried out using FEI Tecnai F30 and JEOL 3000F working at 300 kV. The JEOL 3000F is equipped with an x-ray energy dispersive spectrometer (XEDS).

After 5-revolution HPT processing, the grain sizes of samples at the edge of HPT disks have been refined to a few tens of nanometers. A typical image of the microstructure at the edge of 5-revolution disks is shown in Fig. 1(a), in which equiaxed grains with sizes in the range of ~ 10 nm–50 nm are surrounded by amorphous grain boundaries (GBs) in the form of white contrast in the figure. Amorphous GBs were also found in nanocrystalline CuZn¹⁹ and NiTi²⁰ alloys produced by HPT. Previous investigations reveal that the formation of amorphous GBs is associated with excessive accumulation of dislocations at the original crystalline GBs, and dislocation accumulation introduces significant elastic strain which has been theoretically and experimentally proven to play a critical role in the nucleation of an amorphous structure at dislocation cores.^{19–21} The formation of the amorphous structure effectively releases the high elastic strain and reduces the energy of the system. Twin boundaries, which appear as straight lines, are also seen in some of the nanocrystalline grains, which is a typical feature of SPD nanocrystalline Cu and Cu-Al alloys.^{22,23}

Detailed high-resolution TEM analysis provides clear evidence of elemental separation in some areas of the structure. Figure 1(b) shows a typical high-resolution TEM image of a grain with a size of ~ 40 nm. The grain appears very dark because it is imaged along a $\langle 011 \rangle$ zone axis. In contrast, the amorphous GB area appears bright. Between the dark grain and the bright amorphous GB at the right-hand side of the grain is a narrow grey belt with a width of ~ 2 nm or less. Careful examination of the grey belt area indicates

^{a)}Authors to whom correspondence should be addressed. Electronic addresses: xiaozhou.liao@sydney.edu.au and ytzhu@ncsu.edu

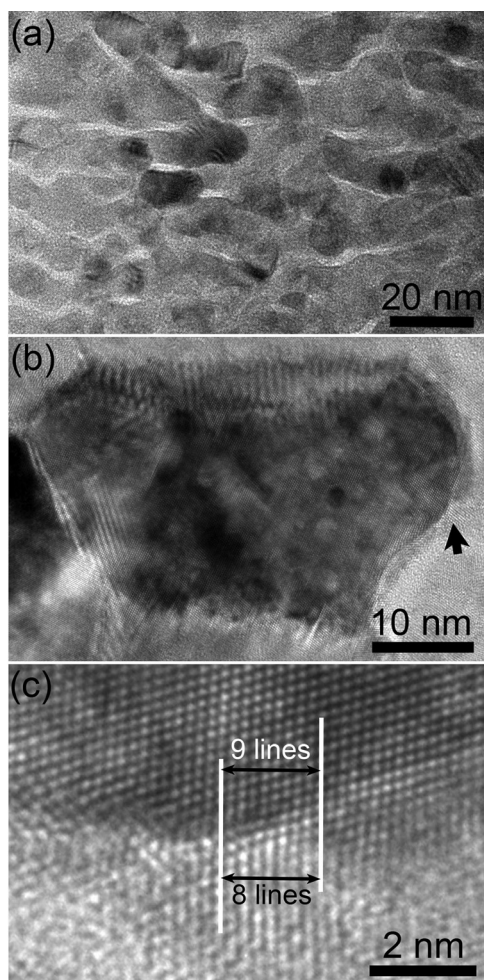


FIG. 1. (a) A typical bright-field TEM image showing a nanocrystalline grain structure. Amorphous GBs with bright contrast are seen surrounding nanocrystalline grains; (b) a high-resolution TEM image of a grain taken from a $\langle 011 \rangle$ zone-axis; (c) a magnified image of the area indicated by an arrow in (b). Two parallel straight lines are drawn in (c).

that the grey belt area is of a crystalline structure with a lattice parameter larger than that of the grain and that some lattice planes in the Cu grain and in the grey area are parallel to each other. Misfit dislocations can be found at the interface of the grain and the grey belt area, indicating that this is a semi-coherent boundary. Part of the belt area, which is indicated by an arrow in Fig. 1(b), is further magnified and shown in Fig. 1(c). Two white lines parallel to a group of $\{111\}$ planes in the grain are drawn in Fig. 1(c). The two white lines are positioned in such a way that there are 8 Cu $\{111\}$ lattice planes and 7 parallel lattice planes in between the two white lines in the Cu grain and the grey area, respectively. In other words, the distance of 9 Cu $\{111\}$ planes is equal to the distance of 8 lattice planes in the grey area. The ratio of 9 over 8, which equals to 1.125, coincides with the ratio (1.122) of the lattice parameters of Al (0.405 nm) and Cu (0.361 nm), indicating that the grey area is the Al phase, which is confirmed by compositional analysis using XEDS. This result indicates that Al is separated from the Cu matrix and precipitated at the interface of Cu grains and the amorphous GBs when the Cu grains are refined to a few tens of nanometers.

It is interesting to note that the degree of the elemental separation increases with reducing Cu grain sizes. Therefore,

the separation can be seen more clearly in finer grains. Fig. 2(a) shows a typical example of this trend. A twinned Cu grain with a grain size of ~ 30 nm is completely surrounded by Al precipitates. The cube-cube orientation relationship is seen in the upper-right and the bottom areas of Fig. 2(a). A magnified image of the upper-right area of Fig. 2(a) is shown in Fig. 2(b) to see the detailed structure of the area. Two parallel lines with an equal length were drawn perpendicular to a group of Cu $\{111\}$ planes. One line falls in the Cu grain and the other line is located in an Al precipitate. Again, when the length of the lines equals to the inter-planar distance of 9 Cu $\{111\}$ planes, it matches the inter-planar distance of 8 Al $\{111\}$ planes, further confirming that the precipitates are Al. Note that the Al/Cu atomic ratio for the grain in Fig. 2 is higher than the nominal composition of CuAl alloys investigated in this work, indicating that the separation was a continuous process during the HPT and grain refinement process and that this resulted in a non-uniform elemental distribution among different areas/grains. Indeed, separation was seen in some nanograins but not in some other nanograins.

In addition to areas in which nanocrystalline grains are surrounded by amorphous GBs, there are also nanocrystalline areas without amorphous GBs. Fig. 3(a) shows a typical image of such areas. High-resolution TEM images do not reveal clear evidence of Al separation at GBs, i.e., an area without amorphous GBs is of only the single Cu (Al) solid solution phase. However, XEDS data indicate that Al separation to the GB area still occurs in the nanocrystalline grains

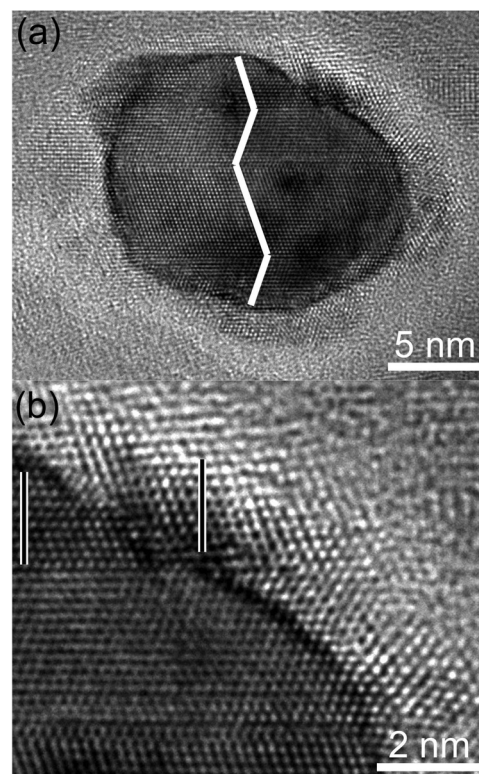


FIG. 2. (a) A high-resolution TEM image of a grain with a size of ~ 20 nm, showing Al separation covering the complete GB. White zig-zag lines in the grain indicate the twin relationship in different parts of the grain; and (b) a magnified image of the upper-right area of (a). Two parallel straight lines are drawn in (b).

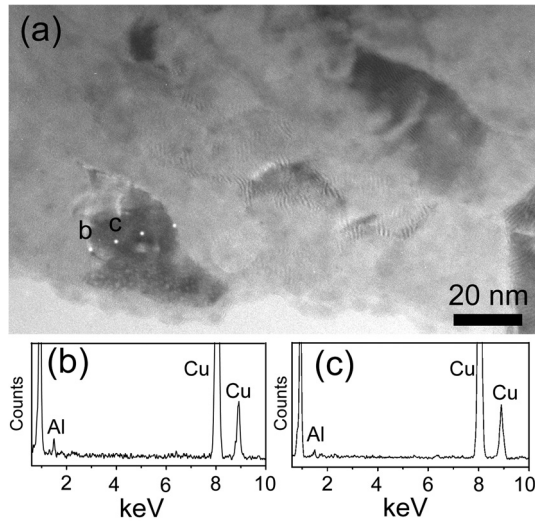


FIG. 3. (a) A typical bright-field image of a nanocrystalline area without amorphous GBs. Four white spots indicate areas where compositional analysis using XEDS was conducted; (b) and (c) show the XEDS data obtained from spots “b” and “c” in (a), respectively.

in such an area. An example of a nanocrystalline grain with a grain size of ~ 30 nm is demonstrated in Fig. 3. XEDS data were collected from four spots in the grain, which are marked with white dots in Fig. 3(a). Two spots are located at GBs while the other two spots are in the grain interior. XEDS data from spots marked with “b” and “c” in Fig. 3(a) are shown in Figs. 3(b) and 3(c), respectively, which clearly shows that the relative intensity of the Al peak at spot “b” is stronger than that at spot “c,” which indicates Al separation to the GB. Similar results were obtained from the other two spots in Fig. 3(a).

In an alloy system in which solutes and solvents are of very different sizes, large substitutional solute elements impose compressive strains in their vicinity. These solute elements tend to diffuse and segregate to areas with tensile strains so as to partially reduce the overall strain energy in the system. This kind of elemental separation has been widely reported in crystalline defects including dislocations and GBs,^{2,24,25} and in strained nanostructures.²⁶ It is expected that excessive lattice (tensile) strain and dislocations exist at the GB areas of the nanocrystalline grains produced by SPD.^{27,28} These strained areas are preferred locations for Al separation. Further, a SPD nanocrystalline material usually has a very high density of vacancy defects,²⁹ which significantly accelerates the diffusion process of substitutional solute atoms. The combined effect of the high (tensile) strains at GBs and a high density of vacancies results in Al separation to the GBs. Experimental results show that Al separation at amorphous GBs (Figs. 1 and 2) is more significant than at crystalline GBs (Fig. 3). This is because the amorphous structure is able to dissipate the strain that would be built up by significant elemental separation at crystalline GBs.

Grain size plays a significant role in the elemental separation process. It is expected that only when the grain size is smaller than a critical value will the elemental separation be possible. This can be explained by the following qualitative thermodynamic analysis of the Gibbs free energy as a function of grain size.

Assuming a spherical grain with a diameter of $2r$ (or a radius of r), its Gibbs free energy before separation (the mixed state) can be expressed as

$$G_m = \frac{4\pi r^3}{3} G_m^0 + \frac{4\pi r^2}{2} \gamma_m, \quad (1)$$

where G_m^0 and γ_m are the volume free energy per unit volume and GB energy per unit area in the mixed state, respectively. Note that the division by 2 in the second term is because each GB is shared by two neighbouring grains.

After separation, a core/shell structure is formed and the grain size remains approximately the same. Assuming the inner Cu core has a radius of r_{Cu} and the Al shell has a thickness of h_{Al} . The following approximations are used for volume calculations: at the early stages of the separation process, because the Al shell has a very small thickness, the radius of the Cu core can be treated as being approximately equal to r , and therefore the volume of the core remains approximately the same as the volume of the original grain size; the volume of the shell can be written as $4\pi r^2 h$ for first-order approximation. The Gibbs free energy after separation can be expressed as

$$G_s = 4\pi r^2 h G_{Al}^0 + \frac{4\pi r^3}{3} G_{Cu}^0 + \frac{4\pi r^2}{2} \gamma_{Al} + 4\pi r^2 \gamma_{Al-Cu}, \quad (2)$$

where G_{Al}^0 , G_{Cu}^0 , γ_{Al} , and γ_{Al-Cu} are the volume free energy per unit volume of the Al shell, the volume free energy per unit volume of the Cu core, GB energy per unit area of the Al shell, and interfacial energy per unit area of the Al-Cu interface, respectively.

Therefore, the total free energy change for the elemental separation is

$$\begin{aligned} \Delta G &= G_s - G_m = 4\pi r^2 h G_{Al}^0 + \frac{4\pi r^3}{3} G_{Cu}^0 + \frac{4\pi r^2}{2} \gamma_{Al} \\ &\quad + 4\pi r^2 \gamma_{Al-Cu} - \frac{4\pi r^3}{3} G_m^0 - \frac{4\pi r^2}{2} \gamma_m \\ &= (G_{Cu}^0 - G_m^0) \frac{4\pi}{3} r^3 + (2hG_{Al}^0 + \gamma_{Al} + 2\gamma_{Al-Cu} - \gamma_m) \frac{4\pi r^2}{2}. \end{aligned} \quad (3)$$

Elemental separation or phase transformation will be possible only when the total free energy change is negative, i.e., $\Delta G < 0$. The critical radius r_c can be calculated by setting $\Delta G = 0$ in Eq. (3)

$$r_c = \frac{3(\gamma_m - 2hG_{Al}^0 - \gamma_{Al} - 2\gamma_{Al-Cu})}{2(G_{Cu}^0 - G_m^0)}. \quad (4)$$

Below the critical value r_c , ΔG is negative, separation is favoured.

From Fig. 1(b), Al separation from the Cu-Al matrix occurs at a grain size as large as ~ 40 nm. Assuming there is only one atomic layer of Al (0.2 nm), which is much smaller than the grain size, at the very beginning of a separation process, the Al shell thickness h in Eq. (4) can be approximately treated as 0. Equation (4) can therefore be further simplified as

$$r_c = -\frac{3\Delta\gamma}{2\Delta G}, \quad (5)$$

where

$$\Delta\gamma = \gamma_{Al} + 2\gamma_{Al-Cu} - \gamma_m \quad (6)$$

and

$$\Delta G = G_{Cu}^0 - G_m^0. \quad (7)$$

It is expected that ΔG is a positive since the mixture of Al and Cu is favoured in large grains. The value of $\Delta\gamma$, which is GB and interfacial energy difference before and after separation, must be negative to make the separation process possible. In other words, the separation process must result in the reduction of total GB and interfacial energy. The larger the $\Delta\gamma$ absolute value, the larger the critical radius r_c and the more significant of the separation phenomenon.

From Eqs. (4) and (5), the critical grain radius r_c depends on the materials properties including Gibbs free energies, GB energies, and interfacial energy between the two elements in a binary system. It is expected that separation will occur only in systems in which the separation will lead to the reduction of the total free energy of the systems. Smaller grain size favours elemental separation not only energetically but also kinetically because the distance needed for the diffusion of a solute atom to a GB is shorter. Furthermore, the excessive amount of vacancies induced by SPD also makes the diffusion of solute atoms very easy.

The phenomenon of elemental separation at GBs in a binary alloy in which the two elements form an equilibrium single-phase solid solution in coarse grains indicates that the available equilibrium phase diagrams of some materials have to be modified when the grain sizes of the materials are reduced to the nanometer regime and are smaller than critical values. Some phase separation phenomena have been reported in the literatures. For example, phase separation occurs in ball-milled FeSn and Fe₂Ge₃ alloys and this was attributed to local melting³⁰ caused by the high energy introduced by ball milling that brings materials into an unstable state, leading to the decomposition of the materials.³¹ This separation mechanism cannot explain the phase separation reported here because the maximum HPT-induced temperature increase was only 120–140 K.³² The HPT-induced temperature increase in the Cu-Al alloys should be much lower than the maximum value because the materials are relatively soft. Deformation-induced nanoscale phase separation in Co-Fe alloys at room temperature was also reported and the possible mechanisms were shear deformation and deformation-enhanced atomic diffusion.³³ It is believed that nanocrystalline grain size also plays a significant role in the separation of Co-Fe although the authors did not claim this. Elemental separation was recently reported in a nanocrystalline W-20 at.% Ti alloy annealed at 1100 °C because of the nanograin sizes although Ti is soluble to 48 at.% in W at the temperature.³⁴ The effect of nanograin size on the elemental separation in the last two systems should be very similar to that in the Cu-Al alloys reported here.

The elemental separation may have significant impact on the properties of nanocrystalline materials. For example, the separation at GBs may pin the boundaries and therefore

improve the thermal stability of the nanocrystalline materials.^{24,35} It may also affect significantly the catalytic performance of nanoparticle catalyst.³⁶ It would be interesting to explore detailed effects of the phenomenon on materials properties including physical, mechanical, and chemical properties. Finally, to design a nanocrystalline alloy with elemental separation, we need to choose an alloy element that produces a large negative $\Delta\gamma$.

In summary, Al separation at GBs occurs in nanocrystalline Cu-Al alloys produced by high-pressure torsion processing. The extent of the separation increases with decreasing grain size, indicating that grain size plays a significant role in the elemental separation, which has been qualitatively explained based on the Gibbs free energy of the nanocrystalline materials.

The authors are grateful for scientific and technical input and support from the Australian Microscopy & Microanalysis Research Facility node at the University of Sydney. The authors would like to thank Dr. C. C. Yang and Professor W. Y. Hu for their helpful discussion. This project was supported by the Australian Research Council [Grant Nos. DP120100510 (X.Z.L.) and DP110103117 (Y.B.W.)], a Grant-in-Aid for Scientific Research from the MEXT, Japan, in Innovative Areas “Bulk Nanostructured Metals” (Z.H.), and the U.S. Army Research Office and Army Research Laboratory (Y.T.Z.).

¹A. P. Zhilyaev and T. G. Langdon, *Prog. Mater. Sci.* **53**, 893 (2008).

²P. V. Liddicoat, X. Z. Liao, Y. T. Zhu, Y. H. Zhao, E. J. Lavernia, M. Y. Murashkin, R. Z. Valiev, and S. P. Ringer, *Nat. Commun.* **1**, 63 (2010).

³X. Z. Liao, J. Y. Huang, Y. T. Zhu, F. Zhou, and E. J. Lavernia, *Philos. Mag.* **83**, 3065 (2003).

⁴Y. B. Wang, J. C. Ho, Y. Cao, X. Z. Liao, H. Q. Li, Y. H. Zhao, E. J. Lavernia, S. P. Ringer, and Y. T. Zhu, *Appl. Phys. Lett.* **94**, 091911 (2009).

⁵X. Z. Liao, A. R. Kilmametov, R. Z. Valiev, H. S. Gao, X. D. Li, A. K. Mukherjee, J. F. Bingert, and Y. T. Zhu, *Appl. Phys. Lett.* **88**, 021909 (2006).

⁶Y. B. Wang, J. C. Ho, X. Z. Liao, H. Q. Li, S. P. Ringer, and Y. T. Zhu, *Appl. Phys. Lett.* **94**, 011908 (2009).

⁷Y. B. Wang, Y. H. Zhao, Q. Lian, X. Z. Liao, R. Z. Valiev, S. P. Ringer, Y. T. Zhu, and E. J. Lavernia, *Scr. Mater.* **63**, 613 (2010).

⁸J. Y. Huang, Y. K. Wu, and H. Q. Ye, *Appl. Phys. Lett.* **66**, 308 (1995).

⁹Y. Ivanisenko, W. Lojkowski, R. Z. Valiev, and H. J. Fecht, *Acta Mater.* **51**, 5555 (2003).

¹⁰G. Sha, Y. B. Wang, X. Z. Liao, Z. C. Duan, S. P. Ringer, and T. G. Langdon, *Acta Mater.* **57**, 3123 (2009).

¹¹C. C. Koch, *Annu. Rev. Mater. Sci.* **19**, 121 (1989).

¹²E. Ma, J. H. He, and P. J. Schilling, *Phys. Rev. B* **55**, 5542 (1997).

¹³A. R. Yavari, P. J. Desre, and T. Benamer, *Phys. Rev. Lett.* **68**, 2235 (1992).

¹⁴S. Odunuga, Y. Li, P. Krasnochtchekov, P. Bellon, and R. S. Averback, *Phys. Rev. Lett.* **95**, 045901 (2005).

¹⁵P. Bellon and R. S. Averback, *Phys. Rev. Lett.* **74**, 1819 (1995).

¹⁶A. C. Lund and C. A. Schuh, *Phys. Rev. Lett.* **91**, 235505 (2003).

¹⁷C. Suryanarayana, *Prog. Mater. Sci.* **46**, 1 (2001).

¹⁸H. Okamoto, *Desk Handbook: Phase Diagram for Binary Alloys* (ASM International, Materials Park, Ohio USA, 2000), p. 29.

¹⁹Y. B. Wang, X. Z. Liao, Y. H. Zhao, E. J. Lavernia, S. P. Ringer, Z. Horita, T. G. Langdon, and Y. T. Zhu, *Mater. Sci. Eng., A* **527**, 4959 (2010).

²⁰J. Y. Huang, Y. T. Zhu, X. Z. Liao, and R. Z. Valiev, *Philos. Mag. Lett.* **84**, 183 (2004).

²¹I. A. Ovid'ko and A. B. Reizis, *J. Phys. D: Appl. Phys.* **32**, 2833 (1999).

²²X. Z. Liao, Y. H. Zhao, S. G. Srinivasan, Y. T. Zhu, R. Z. Valiev, and D. V. Gunderov, *Appl. Phys. Lett.* **84**, 592 (2004).

²³X. H. An, Q. Y. Lin, S. D. Wu, Z. F. Zhang, R. B. Figueiredo, N. Gao, and T. G. Langdon, *Scr. Mater.* **64**, 954 (2011).

- ²⁴Y. Amouyal, S. V. Divinski, L. Klinger, and E. Rabkin, *Acta Mater.* **56**, 5500 (2008).
- ²⁵I. Sabirov, M. Yu. Murashkin, and R. Z. Valiev, *Mater. Sci. Eng., A* **560**, 1 (2013).
- ²⁶X. Z. Liao, J. Zou, D. J. H. Cockayne, R. Leon, and C. Lobo, *Phys. Rev. Lett.* **82**, 5148 (1999).
- ²⁷R. Z. Valiev, R. K. Islamgaliev, and I. V. Alexandrov, *Prog. Mater. Sci.* **45**, 103 (2000).
- ²⁸J. Y. Huang, Y. T. Zhu, H. Jiang, and T. C. Lowe, *Acta Mater.* **49**, 1497 (2001).
- ²⁹M. J. Zehetbauer, G. Steiner, E. Schaffer, A. Korznikov, and E. Korznikova, *Mater. Sci. Forum* **503–504**, 57 (2006).
- ³⁰Y. S. Kwon, J. S. Kim, D. W. Choi, K. B. Gerasimov, and S. S. Avramchuck, *J. Mater. Sci.* **39**, 5213 (2004).
- ³¹P. I. Loeff and H. Bakker, *Europhys. Lett.* **8**, 35 (1989).
- ³²A. P. Zhiyaev, J. M. Garcia-infanta, F. Carreno, T. G. Langdon, and O. A. Ruano, *Scr. Mater.* **57**, 763 (2007).
- ³³L. C. Zhang, M. Calin, F. Paturaud, C. Mickel, and J. Eckert, *Appl. Phys. Lett.* **90**, 201908 (2007).
- ³⁴T. Chookajorn, H. A. Murdoch, and C. A. Schuh, *Science* **337**, 951 (2012).
- ³⁵K. A. Darling, R. N. Chan, P. Z. Wong, J. E. Semones, R. O. Scattergood, and C. C. Koch, *Scr. Mater.* **59**, 530 (2008).
- ³⁶X. Z. Liao, Y. T. Zhu, A. Serquis, D. E. Peterson, and H. F. Xu, *Appl. Phys. Lett.* **82**, 2694 (2003).